Applied Physics Letters

RESEARCH ARTICLE | NOVEMBER 07 2025

Spin-dependent transport in altermagnet CrSb-based magnetic tunnel junction

Yukun Shi ; Guohui Zhan ; Lijun Xu ; Kun Luo ; Jiangtao Liu ; Zhenhua Wu ; Hongwei Liu

Check for updates

Appl. Phys. Lett. 127, 182409 (2025)
https://doi.org/10.1063/5.0278985

View Online
Export Citation

Articles You May Be Interested In

Nonlinear field dependence of Hall effect and high-mobility multi-carrier transport in an altermagnet CrSb

Appl. Phys. Lett. (January 2025)

Dirac edge states as signature of two-dimensional altermagnetic topological crystalline phase

Appl. Phys. Lett. (December 2025)

Tunneling magnetoresistance in altermagnetic tunnel junctions with the half-metal electrode

Appl. Phys. Lett. (August 2025)

11 February 2026 02:08:35

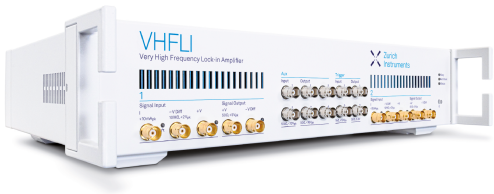

Zurich Instruments

Freedom to Innovate.

The New VHFLI 200 MHz Lock-in Amplifier.

Orchestrate pulses, triggers, and acquisition as the hub of your experiment.
Discover more – run every signal analysis tool, simultaneously.

Order now

AIP Publishing

Applied Physics Letters ARTICLE pubs.aip.org/aip/apl

Spin-dependent transport in altermagnet CrSb-based magnetic tunnel junction

Cite as: Appl. Phys. Lett. **127**, 182409 (2025); doi: 10.1063/5.0278985
Submitted: 5 May 2025 · Accepted: 22 October 2025 ·
Published Online: 7 November 2025

View Online Export Citation CrossMark

Yukun Shi,[1,2] Guohui Zhan,[3,a)] Lijun Xu,[1,2] Kun Luo,[1] Jiangtao Liu,[4] Zhenhua Wu,[3,a)] and Hongwei Liu[1,2,a)]

AFFILIATIONS

[1]Institute of Microelectronics, Chinese Academy of Sciences, 100029 Beijing, China
[2]School of Integrated Circuits, University of Chinese Academy of Sciences, 100029 Beijing, China
[3]School of Physics, Zhejiang University, 310058 Zhejiang, China
[4]School of Mechatronics Engineering, Guizhou Minzu University, Guiyang 550025, China

[a)]Authors to whom correspondence should be addressed: ghzhan@zju.edu.cn; wuzhenhua@zju.edu.cn; and liuhongwei@ime.ac.cn

ABSTRACT

Altermagnetism, an emerging magnetic order state that combines the spin polarization of ferromagnets with the antiferromagnetic resistance to magnetic perturbations, provides a new route to overcome the performance bottleneck of traditional spintronic devices. This Letter focuses on the altermagnetic material CrSb, revealing the spin-polarized band structure protected by real space rotation and mirror operations in the three-dimensional Brillouin zone of CrSb through symmetry analysis and density functional theory calculations, as well as the role of spin–orbit coupling in regulating the degeneracy of the bands. Further, by combining the non-equilibrium Green's function method, we examine the quantum transport properties of altermagnetic CrSb-based magnetic tunnel junction (MTJ). Our results show that the tunneling magnetoresistance (TMR) near the Fermi level reaches 60% for a vacuum barrier of 2.196 Å. When the vacuum is replaced by an *h*-BN monolayer whose effective thickness is 4.4 Å, the TMR decreases to 20%, breaking the limitation of spin-polarized current dependence in traditional ferromagnetic MTJs. The research combined "Néel spin current" and clarified the cooperative transport mechanism of the spin channels of the altermagnetic sublattices. It not only broadens the theoretical framework of altermagnetic materials but also lays an important foundation for the design of spintronic devices based on *g*-wave symmetry altermagnetism.

Published under an exclusive license by AIP Publishing. https://doi.org/10.1063/5.0278985

11 February 2026 02:08:35

Spintronics exploits the spin degree of freedom of electrons in condensed matter for information processing and storage.[1] Most spintronic applications rely on detecting or manipulating highly spin-polarized currents to control magnetic order parameters.[2] A key example is the magnetic tunnel junction (MTJ), where spin-polarized electrons tunnel from one ferromagnetic metal through an insulating barrier into another.[3] The MTJ's conductance depends on the relative magnetization alignment of the two ferromagnetic electrodes, giving rise to the tunneling magnetoresistance (TMR) effect.[4] However, conventional ferromagnetism-based systems are fundamentally constrained by inherent limitations: (i) environmental field sensitivity—external magnetic perturbations destabilize moment orientation; (ii) inter-device dipolar coupling—stray fields from spontaneous magnetization induce crosstalk, severely limiting high-density integration; (iii) inertial domain-wall dynamics—intrinsic sluggishness restricts magnetization manipulation rates, with characteristic switching times hardly exceeding the picosecond regime.[5–7] Recently, studies on the classification of spin group symmetry applicable to collinear magnets have discovered a third basic type of magnetism in addition to ferromagnetism and antiferromagnetism: altermagnetism (AM).[8–10] Its characteristic is unique spin symmetry involving antiparallel sublattices, which are interconnected through specific real space rotation transformations. It has been found that altermagnets exhibit spin splitting on the Fermi surface, leading to spin-polarized currents along certain crystal directions.[11–16] These interesting results indicate that time-reversal symmetry breaking has occurred in this magnet, and some of the predictions have been experimentally validated. These include anomalous Hall effect (AHE),[17–26] magneto-optical Kerr effect[27–29] as well as spin current[10,30–32] and tunneling magnetoresistance.[9,10,13,33–39]

These findings indicate that collinear compensated long-range magnetic ordered magnets are promising candidates for core materials in spintronic devices, thus broadening the material spectrum for

Published under an exclusive license by AIP Publishing

spintronic applications. Altermagnetic materials combine the key features of both ferromagnets and antiferromagnets, exhibiting distinct physical phenomena and promising application potential. They have become a focal point of research in magnetism over recent years. From the perspective of the development of spintronic devices, AM materials possess distinct advantages. Not only do they mitigate the detection challenges inherent to antiferromagnets but also their compensated magnetic configuration reduces the sensitivity to stray magnetic fields compared to ferromagnetic materials, thereby facilitating the development of spintronic devices.

Theoretical studies demonstrate that altermagnetic candidates with specific spin group symmetries can be systematically classified according to their symmetry characteristics (e.g., *d*-, *g*-, and *i*-wave spin splittings), establishing a comprehensive theoretical framework for AM research.[8,9] Experimentally, RuO_2 has been extensively characterized as a prototypical *d*-wave AM material, where time-reversal symmetry breaking-induced electronic responses have been thoroughly elucidated through combined theoretical and experimental investigations, making it a paradigmatic system for studying altermagnetism.[10,30–32,40,41] In addition, angle-resolved photoemission spectroscopy (ARPES) has enabled direct observation of momentum space band splitting and spin polarization in MnTe and $MnTe_2$, providing definitive experimental evidence for the band characteristics of AM materials.[6,10,42–44]

Recently, AM research predominantly focuses on *d*-wave systems, while investigations into the transport properties of *g*-wave AMs remain notably scarce. Compared to their *d*-wave counterparts, *g*-wave AMs exhibit more intricate band structures: the weak band splitting in three-dimensional systems leads to overlapping bands that are challenging to characterize accurately, posing significant obstacles for both theoretical predictions and experimental verification. In this study, we investigate through first-principles quantum transport calculations the application potential of *g*-wave altermagnet CrSb with spin-degenerate Fermi surfaces in AM-MTJs. Based on symmetry analysis, we demonstrate the stable spin-dependent transport phenomena in MTJs with g-wave altermagnet CrSb-based.

The quantum transport of magnetic tunnel junction was calculated using the density functional theory and non-equilibrium Green's function method (DFT+NEGF). The exchange and correlation effects are treated within the generalized gradient approximation (GGA) using the Perdew–Burke–Ernzerhof (PBE) approach.[45] The atomic structure was modeled using QuantumATK, employing the non-relativistic pseudopotential from the Fritz Haber Institute (FHI), with a single-zeta polarized basis set. The calculations involved the use of generalized gradient approximation plus the Hubbard U functional (GGA+U), with $U_{eff} = 1$ eV on the Cr 3d orbitals.[46] The cutoff energy was set to 310 Ry, and a $7 \times 7 \times 151$ k-point grid was used for self-consistent calculations to eliminate the Fermi level (E_F) mismatch between the electrodes and the central region. These parameters achieved a good balance between computational time and accuracy.

As shown in Fig. 1(a), the CrSb crystal possesses a NiAs-type structure (space group $P6_3/mmc$), with lattice parameters $a = b = 4.152$ Å, $c = 5.492$ Å, $\alpha = \beta = 90°$, and $\gamma = 120°$. CrSb has emerged as a highly potential AM candidate material due to its exceptionally high Néel temperature ($T_N > 700$ K), which has garnered extensive attention. Notably, the spin splitting near the Fermi level demonstrates *g*-wave symmetric spin texture (antisymmetric sixfold spin-momentum locking), approximately 1 eV, being more prominent in comparison to other AM candidates.[46,47] Furthermore, the metallic nature of CrSb is conducive for reducing read–write energy consumption and enhancing data stability, laying a robust foundation for its further application in spintronic devices. In the ground state, the magnetic moments of CrSb are arranged in a collinear compensated magnetic order, manifesting a state analogous to A-type collinear antiferromagnetism, with the Néel vectors aligned along the c axis. Each Cr atom is surrounded by six Sb atoms, forming two distinct sublattices with opposite spins [distinguished by red and blue colors in Fig. 1(b)].

We have conducted an elaborate analysis of the band structure in both the high-symmetry and low-symmetry regions of the three-dimensional Brillouin zone. In the absence of spin–orbit coupling, the calculated crystal bands undergo spin degeneracy along the Γ–M–L–K–A–L path [Figs. 1(c) and 1(d)]. Nevertheless, a pair of bands with opposite spins can be observed, which are degenerate at the Γ, L, and L′ points but split when departing from these high-symmetry points, forming antisymmetric band lines with a spin splitting of approximately 1 eV, where black (red) represents the spin-up (spin-down) state. Additionally, it is noted that CrSb possesses a spin-polarized quasiparticle that is fourfold degenerate at the Γ point and exhibits significant spin splitting commencing from this point.

The ARPES measurements exhibit excellent agreement with the calculations based on density functional theory.[47–50] A prominent Kramer degeneracy was observed at the high-symmetry positions in the momentum space, while distinct features of AM-induced band splitting were captured outside these high-symmetry positions. The experimental results indicate that there exists a band splitting of up to 0.93 eV near the Fermi level,[47–50] which is the maximum value observed hitherto among all confirmed AM materials. On the other hand, the bulk *g*-wave-like AM existing in CrSb can be clearly identified [Fig. 1(f)], which substantiates the *g*-wave symmetry characteristics of CrSb as a typical AM material.

These discoveries not only highlight CrSb as an ideal candidate for investigating the properties of AM materials, but also accentuate its potential applications in spintronics. Hence, we have summarized the spin polarization characteristics of CrSb within the Γ–A–L–M plane. Further computations reveal the minute discrepancies in spin splitting in the presence and absence of spin–orbit coupling, as shown in Figs. 1(d) and 1(e). Specifically, when SOC is taken into account, the energy band exhibits a smaller bandgap within the Γ–A–L–M plane, and the originally fourfold degenerate band at the Γ point splits into a more sophisticated structure due to the effect of orbital coupling, in good agreement with previous literature reports.[47,48]

To explore the potential application of the *g*-wave AM material CrSb in spintronic devices, we initially examined the conductance properties of magnetic tunnel junctions. In the absence of SOC, the conductance G^σ per unit area along the transmission direction (*z*-axis) can be computed via two spin components,

$$G^\sigma(E) = \frac{e^2}{h}\sum_{k_{||}} T^\sigma\left(\vec{k}_{||}, E\right) = \frac{e^2}{h}\sum_{k_{||}} T^{up}\left(\vec{k}_{||}, E\right) + T^{down}\left(\vec{k}_{||}, E\right), \tag{1}$$

11 February 2026 02:08:35

Published under an exclusive license by AIP Publishing

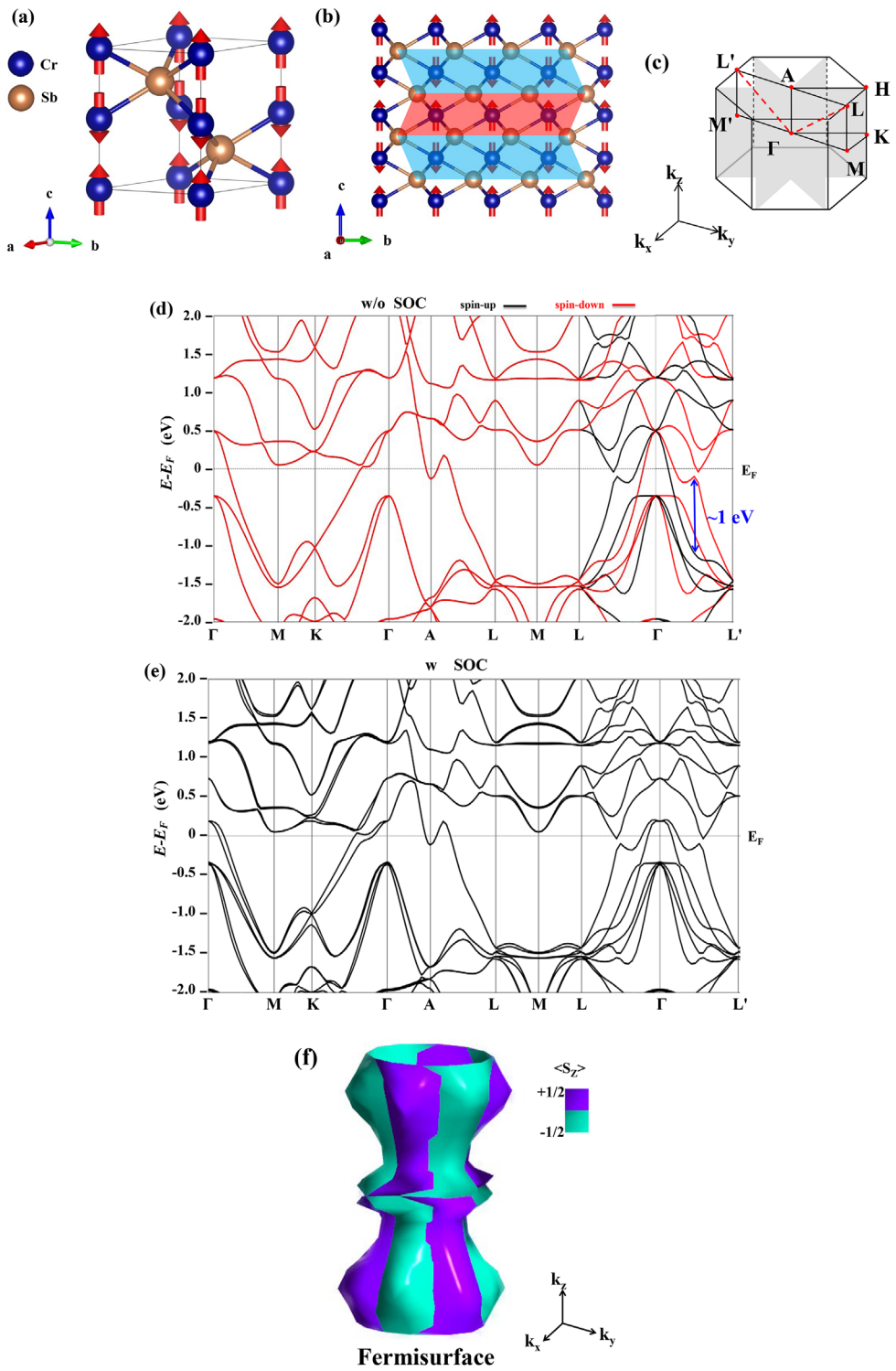

FIG. 1. The crystal structure and electronic properties of CrSb. (a) The unit cell of CrSb. Its spins are located at the Cr site along the c axis. (b) Stack structures of the spin sublattice of CrSb. (c) In the three-dimensional Brillouin zone of CrSb, red dots represent high-symmetry points. (d) Bulk bands without SOC along the high-symmetry paths, as determined by DFT calculation. Spin splitting bands without SOC along L′–Γ–L (black line and red line) ($k_y = \mp 2\sqrt{3}\pi/3a$, $k_z = \pi/c$), and (e) bulk bands with SOC along the high-symmetry paths. (f) The calculated 3D Fermi surface of the *g*-wave-type CrSb.

11 February 2026 02:08:35

Published under an exclusive license by AIP Publishing

$$T^{\sigma}\left(\vec{k}_{||}, \mathrm{E}\right) = \frac{\hbar}{2}\sum_{n}\int |v_{nz}^{\sigma}| \frac{\partial f}{\partial E_{n}^{\sigma}(\vec{k})} dk_{z}. \quad (2)$$

Herein, $T^{\sigma}(\vec{k}_{||}, E)$ denotes the k-resolved transmission coefficient across the two-dimensional Brillouin zone, where σ represents the spin components of up and down, $|v_{nz}^{\sigma}|$ is the n-th band velocity along the transmission z direction, E_n^{σ} is energy for the n-th band, f is the Fermi distribution function. $T^{up}(\vec{k}_{||}, E)$ and $T^{down}(\vec{k}_{||}, E)$ are respectively the transmission coefficients of the two-dimensional Brillouin zone for spin-up and spin-down sates.

The TMR of MTJs serves as a crucial indicator for assessing the transmission performance of the devices. The core lies in the relative orientation of the magnetization directions of the two magnetic layers, namely whether they are parallel or antiparallel. If T_P indicates the total transmission quantity when the device is in the parallel magnetization direction state, and T_{AP} represents the total transmission quantity when the magnetization directions are antiparallel,

$$\begin{aligned} T_P &= \sum_{k_{||}} T_P^{up}\left(\vec{k}_{||}, E\right) + T_P^{down}\left(\vec{k}_{||}, E\right), \\ T_{AP} &= \sum_{k_{||}} T_{AP}^{up}\left(\vec{k}_{||}, E\right) + T_{AP}^{down}\left(\vec{k}_{||}, E\right). \end{aligned} \quad (3)$$

At this juncture, the TMR ratio of AM-MTJ is defined as

$$TMR = \frac{G_P - G_{AP}}{G_{AP}} \times 100\% = \frac{T_P - T_{AP}}{T_{AP}} 100\%. \quad (4)$$

To explore the potential of altermagnets as the functional core of MTJs and to investigate how their sublattice spin-polarized tunneling channels influence spin transport, we design an AM-MTJ structure CrSb $(10\bar{1}0)$/Δ/CrSb $(10\bar{1}0)$, where Δ represents the vacuum layer). This structure comprises two electrodes, namely the magnetic fixed layer and the magnetic free layer, each consisting of 4 CrSb layers stacked along the CrSb $(10\bar{1}0)$ plane and separated by a vacuum layer, as depicted in Fig. 2(a). The CrSb $(10\bar{1}0)$/Δ/CrSb $(10\bar{1}0)$ structure in Fig. 2(a) is then used as the scattering region of the AM-MTJ connected to two semi-infinite CrSb $(10\bar{1}0)$ electrodes for calculating transmission. Supposing that the spin-polarized conduction channels of the altemagnet along the out-of-plane transmission direction are controlled by sublattices with opposite spins, the functionality of AM-MTJs is contingent upon the relative orientation of the Néel vectors of the two altermagnetic electrodes. For Δ = 2.196 Å, we computed the energy functions and transmission characteristics of AM-MTJs in the Néel vector parallel (P) and antiparallel (AP) states as illustrated in Fig. 2(b). The results suggest that within the calculated energy window, irrespective of the energy and barrier variations, the total transmission

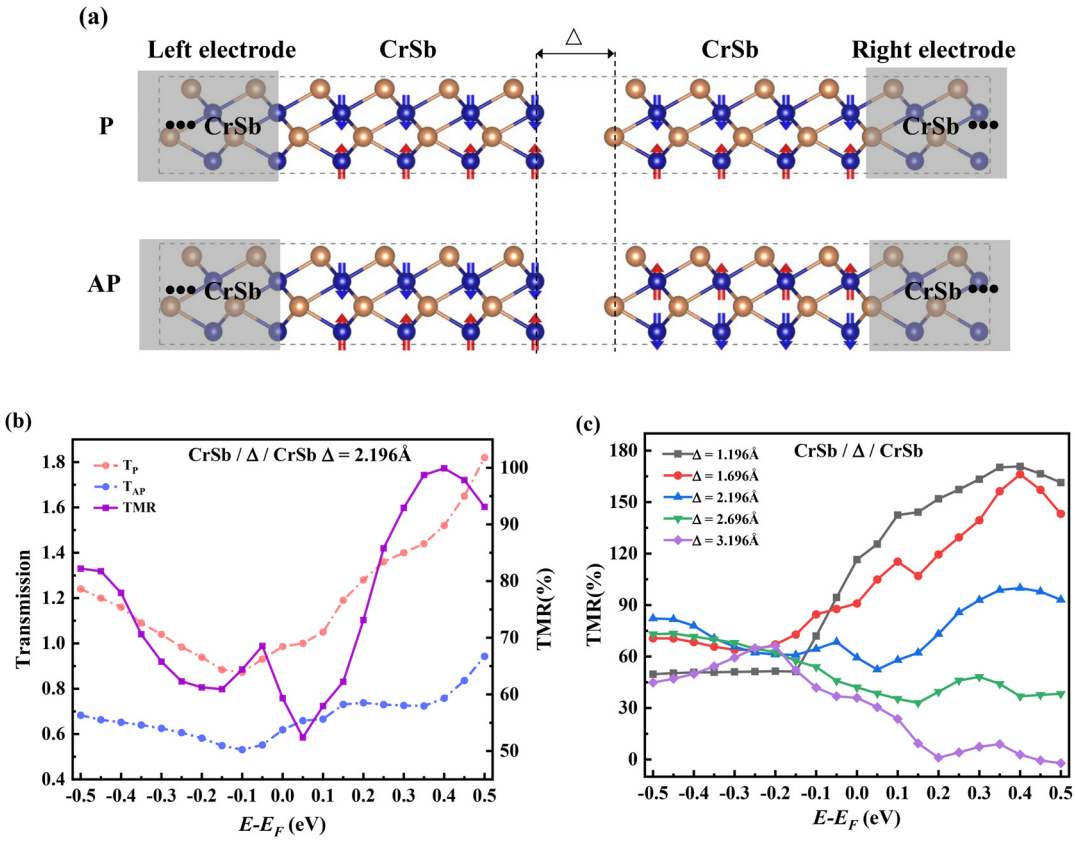

FIG. 2. (a) Atomic structure of a CrSb/Δ/CrSb supercell. The arrows in (a) indicate the magnetic moments of Cr atoms, and a vacuum layer (denoted by Δ). (b) Total transmission and TMR as a function of energy for the AM-MTJ in P (red dots) and AP (blue dots) states. (c) The relationship between TMR and energy corresponding to various distances of vacuum layers.

11 February 2026 02:08:35

Published under an exclusive license by AIP Publishing

in the P state (T_P) is consistently greater than that in the AP state (T_{AP}). This is because in the parallel configuration, the spin-polarized conduction channels formed by the Cr atom sublattices with the same spin direction in the electrodes are matched, resulting in a low-resistance state, while in the anti-parallel arrangement, the spin-up and spin-down channels are mutually blocked, leading to a marked reduction in the spin-up and spin-down transmission rates. Furthermore, we calculated the relationship between TMR and energy when $\Delta = 2.196$ Å. The results indicated that in the vicinity of the Fermi level, the TMR ratio $(T_P - T_{AP})/T_{AP}$ is ~60% for CrSb $(10\bar{1}0)$/Δ/CrSb $(10\bar{1}0)$ AM-MTJs. Additionally, we discovered that in the vicinity of the Fermi level, especially in the energy window where $E - E_F > 0eV$, the TMR ratio of CrSb $(10\bar{1}0)$/Δ/CrSb $(10\bar{1}0)$ gradually diminishes as the thickness of the vacuum layer increases [see Fig. 2(c)]. This is associated with the attenuation of spin polarization of the spin current in the sublattice layer as it traverses the vacuum layer with an increasing distance, indicating that the altermagnetic layer acting as the free layer has difficulty maintaining a pronounced spin polarization effect at a greater distance.

To visually demonstrate this phenomenon more explicitly, we plot the k-resolved transmission function at $E - E_F = 0$ eV [see Fig. 3(a)]. The results reveal that the transmission intensity of the P state is conspicuously higher than that of the AP state. Nevertheless, within both the P state and the AP state, the transmission intensities of spin-up and spin-down channels of the same state remain invariant. This indicates that the device as a whole remains in a spin-neutral current state, which is significantly distinct from the traditional magnetic tunnel junctions with ferromagnetic materials as the core that output spin-polarized currents. Further, we plot the spin-resolved projected local density of states (PLDOS) along the z direction in the P and AP configurations [Fig. 3(b)]. The density of states of the P-state channel attains the maximum value, suggesting that the channel possesses low resistance. By contrast, the density of states of the AP-state channel is lower than that of the P state, indicating a higher resistance.

Based on the phenomena described above, we have constructed a simplified model to elucidate the underlying mechanism.[51] As depicted in Figs. 4(a) and 4(b), when the polarization directions of the left and right altermagnetic layers are perfectly congruent, the spin-up electron transmission channels of the left altermagnetic layer align with those of the right altermagnetic layer. Simultaneously, the spin-down electron transmission channels of the left altermagnetic layer also correspond to those of the right altermagnetic layer, thereby presenting a low-resistance state. Conversely, as depicted in Figs. 4(c) and 4(d), when the polarization direction of the right altermagnetic layer is reversed, the spin channels on both sides fail to match, giving rise to a high-resistance state. Nevertheless, in practical circumstances, since the sublattices constitute an integrated entity, as the ballistic

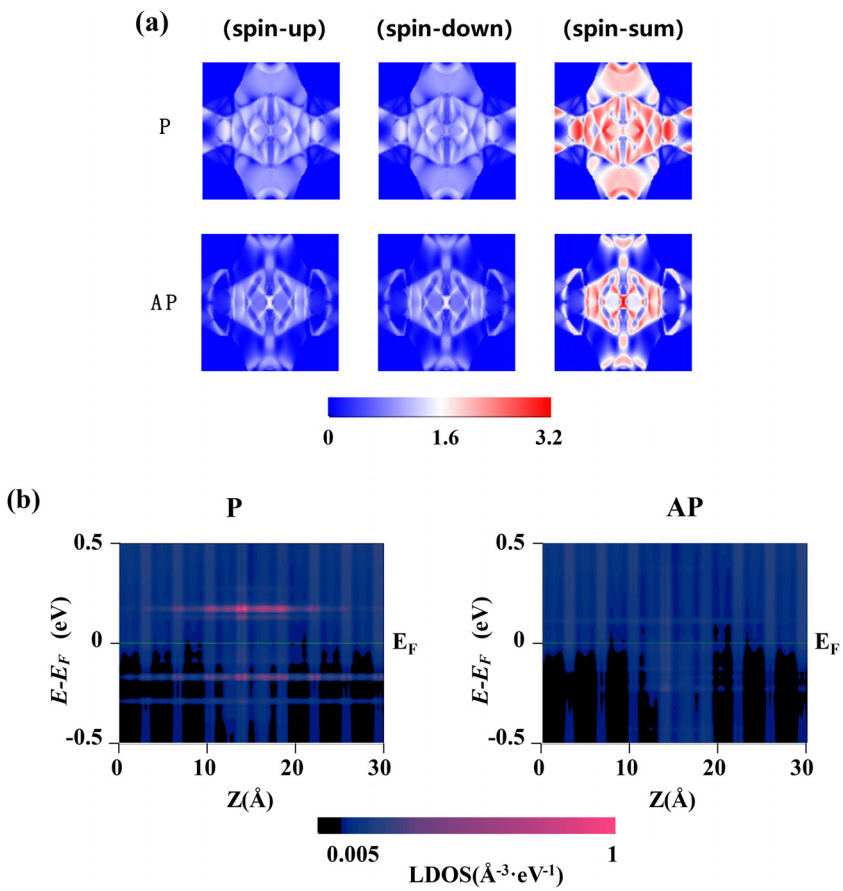

FIG. 3. (a) $k_{||}$-resolved electron transmission distribution T(kx, ky, E = 0 eV) of two magnetic tunnel junctions (MTJs) for spin-up and spin-down channels in P and AP configurations. (b) Projected local density of states (PLDOS) along the transport direction of P and AP configurations.

11 February 2026 02:08:35

Published under an exclusive license by AIP Publishing

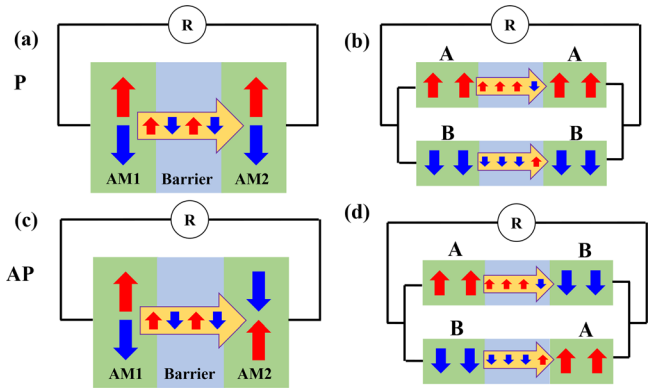

FIG. 4. Schematic illustration of the collinear AM-MTJs constituted by sublattices A and B, wherein the altermagnet can be construed as a resistor and is connected in parallel with the two sublattices (Left and right non-magnetic electrodes are not depicted). (a) P configuration corresponding (b) spin channels on both sides align, enabling efficient transmission; (c) AP configuration corresponding (d) spin channels are mismatched, resulting in suppressed transmission.

transmission distance augments, the interaction among electrons leads to gradual attenuation of the spin polarization intensity with increase in the vacuum layer thickness.

To broaden the applicability of *g*-wave-AM CrSb, we selected *h*-BN as a suitable barrier material for this tunnel junction. Similar to CrSb, *h*-BN also crystallizes in the hexagonal crystal system, with a space group of $P6_3/mmc$, and possesses a two-dimensional layered configuration similar to graphite, manifesting an exceptionally high thermal stability. The lattice parameters of *h*-BN are $a = b = 2.51$ Å, $c = 7.71$ Å, $\alpha = \beta = 90°$, and $\gamma = 120°$. As depicted in Fig. 5(b), the two-dimensional material *h*-BN possesses an indirect bandgap of 5.797 eV, making it an excellent high-temperature insulating material.

We design an AM-MTJ structure CrSb $(10\bar{1}0)$/*h*-BN (0001)/CrSb $(10\bar{1}0)$, as illustrated in Fig. 6(a). Taking into account the effective transmission distance of the spin-polarized current, the center of the magnetic tunnel junction we designed encompasses a solitary *h*-BN layer, with 4 CrSb layers on each side. Owing to the identical space group and closely matched lattice parameters of *h*-BN and CrSb, the lattice mismatch rate of the magnetic tunnel junction constructed along the CrSb $(10\bar{1}0)$ plane is as low as 4%. Selecting *h*-BN as the barrier layer not only boosts the spin injection efficiency of magnetic materials by virtue of its filtering effect on spin electrons but also mitigates the interface stress at the heterointerface on account of the shared crystal system. By calculating the total energy of the system, we determined that the most stable heterojunction spacing is 2.2 Å. Similarly, the CrSb $(10\bar{1}0)$/*h*-BN (0001)/CrSb $(10\bar{1}0)$ structure in Fig. 6(a) is then used as the scattering region of the AM-MTJ connected to two semi-infinite CrSb $(10\bar{1}0)$ electrodes for transmission calculations. We set the magnetic moments in the parallel and antiparallel states of the Néel vector. The figure presents the calculated outcomes of the energy function and transmission characteristics of these AM-MTJs in the parallel and antiparallel states of the Néel vector. The results reveal that within the calculated energy window, irrespective of the energy and barrier, the total transmission of the P state is always greater than that of the AP state. In the vicinity of the Fermi level, the TMR value of the CrSb $(10\bar{1}0)$/*h*-BN (0001)/CrSb $(10\bar{1}0)$ AM-MTJ reaches approximately 20%. Such TMR values are unexpected because the sum of the true spatial distances on both sides of *h*-BN is 4.4 Å. Furthermore, in order to compare the differences between the magnetic tunnel junctions with and without h-BN, we calculated CrSb $(10\bar{1}0)/\Delta$/CrSb $(10\bar{1}0)$ the relationship between TMR and energy when $\Delta = 4.4$ Å [see Fig. 6(b) (green dots)]. At $E - E_F > 0.2$ eV, $TMR < 0$, indicating that near the Fermi level, the MTJ with vacuum layer spacing of $\Delta = 4.4$ Å loses its ability to distinguish between the high- and low-resistance states of the P and AP configurations any longer. This highlights that the application of *h*-BN significantly extends the effective range for maintaining local spin polarization flow within the strongly coupled crystal.

In summary, we have conducted a comprehensive study of the band structure of the altermagnet CrSb, revealing an intricate spin-splitting behavior that underpins its unique electronic properties. Through density functional theory computations, we have confirmed that CrSb exhibits one of the most prominent spin splittings and the highest Néel temperature among known altermagnets. The presence of distinct non-relativistic spin splitting and spin-polarized bands near the Fermi level in CrSb underscores its strong potential for magnetic tunnel junction applications. The concept of spin channels arising from altermagnetic sublattices provides a different perspective on electron transmission in altermagnets and highlights phenomena that are crucial for advancing spintronic technologies. Our study demonstrates that the presence of these spin channels of altermagnetic sublattices gives rise to a substantial tunneling magnetoresistance effect. Overall, our findings reveal the promising role of *g*-wave CrSb altermagnets in magnetic tunnel junction applications, an area that has been largely unexplored until now.

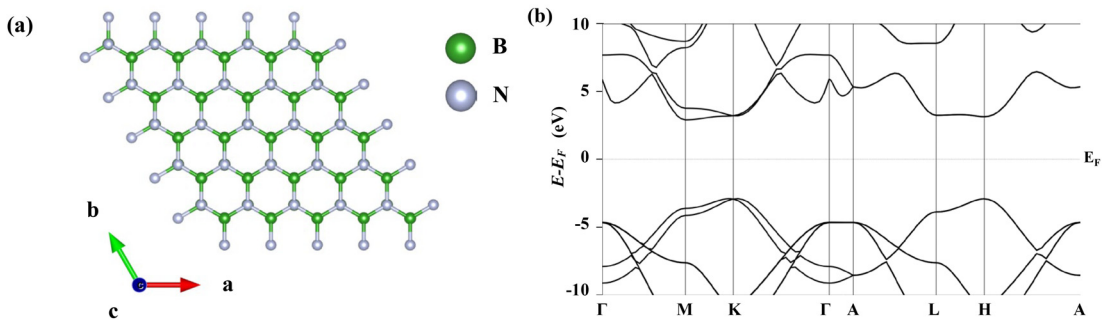

FIG. 5. Crystal and electronic structure of *h*-BN. (a) The crystal structure and (b) the band structure of *h*-BN.

11 February 2026 02:08:35

Published under an exclusive license by AIP Publishing

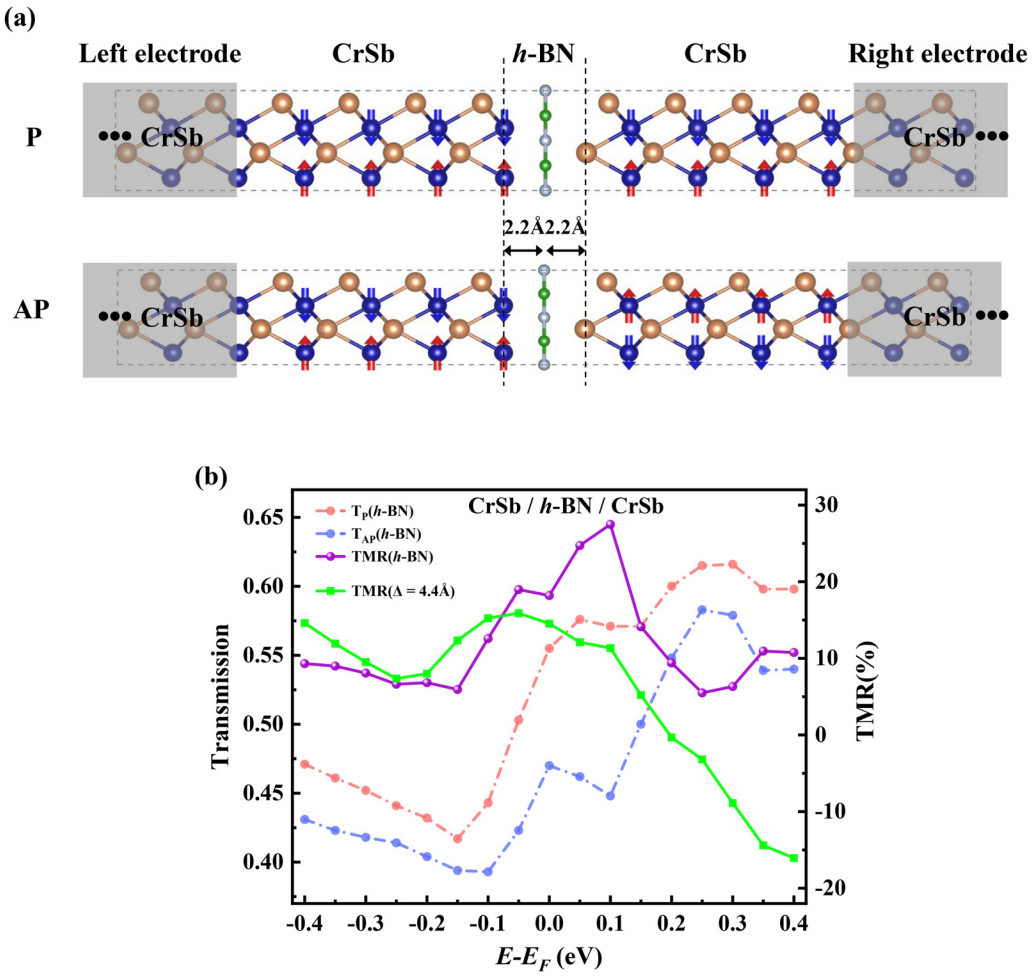

FIG. 6. Structure and TMR for CrSb/*h*-BN/CrSb AM-MTJ devices. (a) Atomic structure of a CrSb/*h*-BN/CrSb supercell. The arrows in (a) indicate the magnetic moments of Cr atoms. (b) Total transmission and TMR as a function of energy for the AM-MTJ in P (red dots) and AP (blue dots) states.

This work was supported in part by the National Natural Science Foundation of China (Grant No. 12174423).

AUTHOR DECLARATIONS

Conflict of Interest

The authors have no conflicts to disclose.

Author Contributions

Yukun Shi: Data curation (equal); Formal analysis (equal); Methodology (equal); Writing – original draft (equal); Writing – review & editing (equal). **Guohui Zhan:** Data curation (equal); Formal analysis (equal); Methodology (equal); Writing – review & editing (equal). **Lijun Xu:** Formal analysis (equal); Methodology (equal). **Kun Luo:** Resources (equal); Software (equal). **Jiangtao Liu:** Software (equal). **Zhenhua Wu:** Resources (equal); Software (equal); Writing – review & editing (equal). **Hongwei Liu:** Data curation (equal); Formal analysis (equal); Methodology (equal); Writing – review & editing (equal).

DATA AVAILABILITY

The data that support the findings of this study are available from the corresponding authors upon reasonable request.

REFERENCES

[1] I. Zutic, *Spintronics Handbook: Spin Transport and Magnetism* (CRC Press/Taylor & Francis Group, 2019).
[2] M. Julliere, "Tunneling between ferromagnetic films," Phys. Lett. A **54**(3), 225–226 (1975).
[3] J. S. Moodera, L. R. Kinder, T. M. Wong, and R. Meservey, "Large magnetoresistance at room temperature in ferromagnetic thin film tunnel junctions," Phys. Rev. Lett. **74**(16), 3273 (1995).
[4] E. Y. Tsymbal, O. N. Mryasov, and P. R. LeClair, "Spin-dependent tunnelling in magnetic tunnel junctions," J. Phys. **15**(4), R109–R142 (2003).
[5] R. Cheng, M. W. Daniels, J. G. Zhu, and D. Xiao, "Ultrafast switching of antiferromagnets via spin-transfer torque," Phys. Rev. B **91**(6), 064423 (2015).
[6] Y. P. Zhu, X. Chen, X. R. Liu, Y. Liu, P. Liu, H. Zha, G. Qu, C. Hong, J. Li, Z. Jiang, X.-M. Ma, Y.-J. Hao, M.-Y. Zhu, W. Liu, M. Zeng, S. Jayaram, M. Lenger, J. Ding, S. Mo, K. Tanaka, M. Arita, Z. Liu, M. Ye, and D. Shen *et al.*,

11 February 2026 02:08:35

Published under an exclusive license by AIP Publishing

"Observation of plaid-like spin splitting in a noncoplanar antiferromagnet," Nature **626**(7999), 523–528 (2024).
[7]A. Hirohata, K. Yamada, Y. Nakatani, I. L. Prejbeanu, B. Diény, P. Pirro, and B. Hillebrands, "Review on spintronics: Principles and device applications," J. Magn. Magn. Mater. **509**, 166711 (2020).
[8]L. Šmejkal, J. Sinova, and T. Jungwirth, "Beyond conventional ferromagnetism and antiferromagnetism: A phase with nonrelativistic spin and crystal rotation symmetry," Phys. Rev. X **12**(3), 031042 (2022).
[9]L. Šmejkal, J. Sinova, and T. Jungwirth, "Emerging research landscape of altermagnetism," Phys. Rev. X **12**(4), 040501 (2022).
[10]R. González-Hernández, L. Šmejkal, K. Výborný, Y. Yahagi, J. Sinova, T. Jungwirth, and J. Železný, "Efficient electrical spin splitter based on nonrelativistic collinear antiferromagnetism," Phys. Rev. Lett. **126**(12), 127701 (2021).
[11]K. H. Ahn, A. Hariki, K. W. Lee, and J. Kuneš, "Antiferromagnetism in RuO_2 as *d*-wave Pomeranchuk instability," Phys. Rev. B **99**(18), 184432 (2019).
[12]S. Hayami, Y. Yanagi, and H. Kusunose, "Momentum-dependent spin splitting by collinear antiferromagnetic ordering," J. Phys. Soc. Jpn. **88**(12), 123702 (2019).
[13]M. Naka, S. Hayami, H. Kusunose, Y. Yanagi, Y. Motome, and H. Seo, "Spin current generation in organic antiferromagnets," Nat. Commun. **10**(1), 4305 (2019).
[14]L. D. Yuan, Z. Wang, J. W. Luo, E. I. Rashba, and A. Zunger, "Giant momentum-dependent spin splitting in centrosymmetric low-*Z* antiferromagnets," Phys. Rev. B **102**(1), 014422 (2020).
[15]S. Hayami, Y. Yanagi, and H. Kusunose, "Bottom-up design of spin-split and reshaped electronic band structures in antiferromagnets without spin-orbit coupling: Procedure on the basis of augmented multipoles," Phys. Rev. B **102**(14), 144441 (2020).
[16]L. D. Yuan, Z. Wang, J. W. Luo, and A. Zunger, "Prediction of low-Z collinear and noncollinear antiferromagnetic compounds having momentum-dependent spin splitting even without spin-orbit coupling," Phys. Rev. Mater. **5**(1), 014409 (2021).
[17]N. Nagaosa, J. Sinova, S. Onoda, A. H. MacDonald, and N. P. Ong, "Anomalous Hall effect," Rev. Mod. Phys. **82**(2), 1539–1592 (2010).
[18]H. Chen, Q. Niu, and A. H. MacDonald, "Anomalous Hall effect arising from noncollinear antiferromagnetism," Phys. Rev. Lett. **112**(1), 017205 (2014).
[19]S. Nakatsuji, N. Kiyohara, and T. Higo, "Large anomalous Hall effect in a non-collinear antiferromagnet at room temperature," Nature **527**(7577), 212–215 (2015).
[20]L. Šmejkal, R. González-Hernández, T. Jungwirth, and J. Sinova, "Crystal time-reversal symmetry breaking and spontaneous Hall effect in collinear antiferromagnets," Sci. Adv. **6**(23), eaaz8809 (2020).
[21]Z. Feng, X. Zhou, L. Šmejkal, L. Wu, Z. Zhu, H. Guo, R. González-Hernández, X. Wang, H. Yan, P. Qin, X. Zhang, H. Wu, H. Chen, Z. Meng, L. Liu, Z. Xia, J. Sinova, T. Jungwirth, and Z. Liu, "An anomalous Hall effect in altermagnetic ruthenium dioxide," Nat. Electron. **5**(11), 735–743 (2022).
[22]I. Sodemann and L. Fu, "Quantum nonlinear Hall effect induced by Berry curvature dipole in time-reversal invariant materials," Phys. Rev. Lett. **115**(21), 216806 (2015).
[23]Z. Z. Du, H. Z. Lu, and X. C. Xie, "Nonlinear Hall effects," Nat. Rev. Phys. **3**(11), 744–752 (2021).
[24]D. F. Shao, S. H. Zhang, G. Gurung, W. Yang, and E. Y. Tsymbal, "Nonlinear anomalous Hall effect for Néel vector detection," Phys. Rev. Lett. **124**(6), 067203 (2020).
[25]H. Liu, J. Zhao, Y. X. Huang, W. Wu, X. L. Sheng, C. Xiao, and S. A. Yang, "Intrinsic second-order anomalous Hall effect and its application in compensated antiferromagnets," Phys. Rev. Lett. **127**(27), 277202 (2021).
[26]C. Wang, Y. Gao, and D. Xiao, "Intrinsic nonlinear Hall effect in antiferromagnetic tetragonal CuMnAs," Phys. Rev. Lett. **127**(27), 277201 (2021).
[27]K. Samanta, M. Ležaić, M. Merte, F. Freimuth, S. Blügel, and Y. Mokrousov, "Crystal Hall and crystal magneto-optical effect in thin films of $SrRuO_3$," J. Appl. Phys. **127**(21), 213904 (2020).
[28]M. Naka, S. Hayami, H. Kusunose, Y. Yanagi, Y. Motome, and H. Seo, "Anomalous Hall effect in κ-type organic antiferromagnets," Phys. Rev. B **102**(7), 075112 (2020).
[29]X. Zhou, W. Feng, X. Yang, G. Y. Guo, and Y. Yao, "Crystal chirality magneto-optical effects in collinear antiferromagnets," Phys. Rev. B **104**(2), 024401 (2021).
[30]A. Bose, N. J. Schreiber, R. Jain, D. F. Shao, H. P. Nair, J. Sun, X. S. Zhang, D. A. Muller, E. Y. Tsymbal, D. G. Schlom, and D. C. Ralph, "Tilted spin current generated by the collinear antiferromagnet ruthenium dioxide," Nat. Electron. **5**(5), 267–274 (2022).
[31]H. Bai, L. Han, X. Y. Feng, Y. J. Zhou, R. X. Su, Q. Wang, L. Y. Liao, W. X. Zhu, X. Z. Chen, F. Pan, X. L. Fan, and C. Song, "Observation of spin splitting torque in a collinear antiferromagnet RuO_2," Phys. Rev. Lett. **128**(19), 197202 (2022).
[32]S. Karube, T. Tanaka, D. Sugawara, N. Kadoguchi, M. Kohda, and J. Nitta, "Observation of spin-splitter torque in collinear antiferromagnetic RuO_2," Phys. Rev. Lett. **129**(13), 137201 (2022).
[33]M. Naka, Y. Motome, and H. Seo, "Perovskite as a spin current generator," Phys. Rev. B **103**(12), 125114 (2021).
[34]H. Y. Ma, M. Hu, N. Li, J. Liu, W. Yao, J. F. Jia, and J. Liu, "Multifunctional antiferromagnetic materials with giant piezomagnetism and noncollinear spin current," Nat. Commun. **12**(1), 2846 (2021).
[35]D. F. Shao, S. H. Zhang, M. Li, C. B. Eom, and E. Y. Tsymbal, "Spin-neutral currents for spintronics," Nat. Commun. **12**(1), 7061 (2021).
[36]B. Chi, L. Jiang, Y. Zhu, G. Yu, C. Wan, J. Zhang, and X. Han, "Crystal-facet-oriented altermagnets for detecting ferromagnetic and antiferromagnetic states by giant tunneling magnetoresistance," Phys. Rev. Appl. **21**(3), 034038 (2024).
[37]B. Chi, L. Jiang, Y. Zhu, G. Yu, C. Wan, and X. Han, "Anisotropic spin filtering by an altermagnetic barrier in magnetic tunnel junctions," Phys. Rev. Appl. **23**(1), 014013 (2025).
[38]L. Zhang, G. Ni, J. He, and G. Gao, "Above room temperature multiferroic tunnel junction with the altermagnetic metal CrSb," Phys. Rev. B **112**(6), 064401 (2025).
[39]W. Sun, M. Wang, B. Sa, S. Dong, and C. Autieri, "Altermagnetizing the FeSe-like two-dimensional materials and approaching to giant tunneling magnetoresistance with Janus Cr4BN (B2) MBene electrode," arXiv:2502.03165 (2025).
[40]L. Šmejkal, A. B. Hellenes, R. González-Hernández, J. Sinova, and T. Jungwirth, "Giant and tunneling magnetoresistance in unconventional collinear antiferromagnets with nonrelativistic spin-momentum coupling," Phys. Rev. X **12**(1), 011028 (2022).
[41]S. Lee, S. Lee, S. Jung, J. Jung, D. Kim, Y. Lee, B. Seok, J. Kim, B. Gyu Park, L. Šmejkal, C.-J. Kang, and C. Kim, "Broken Kramers degeneracy in altermagnetic MnTe," Phys. Rev. Lett. **132**(3), 036702 (2024).
[42]J. Krempaský, L. Šmejkal, S. W. D'souza, M. Hajlaoui, G. Springholz, K. Uhlířová, F. Alarab, P. C. Constantinou, V. Strocov, D. Usanov, W. R. Pudelko, R. González-Hernández, A. Birk Hellenes, Z. Jansa, H. Reichlová, Z. Šobáň, R. D. Gonzalez Betancourt, P. Wadley, J. Sinova, D. Kriegner, J. Minár, J. H. Dil, and T. Jungwirth, "Altermagnetic lifting of Kramers spin degeneracy," Nature **626**(7999), 517–522 (2024).
[43]T. Osumi, S. Souma, T. Aoyama, K. Yamauchi, A. Honma, K. Nakayama, T. Takahashi, K. Ohgushi, and T. Sato, "Observation of a giant band splitting in altermagnetic MnTe," Phys. Rev. B **109**(11), 115102 (2024).
[44]M. Hajlaoui, S. Wilfred D'Souza, L. Šmejkal, D. Kriegner, G. Krizman, T. Zakusylo, N. Olszowska, O. Caha, J. Michalička, J. Sánchez-Barriga, A. Marmodoro, K. Výborný, A. Ernst, M. Cinchetti, J. Minar, T. Jungwirth, and G. Springholz, "Temperature dependence of relativistic valence band splitting induced by an altermagnetic phase transition," Adv. Mater. **36**(31), 2314076 (2024).
[45]J. P. Perdew, K. Burke, and M. Ernzerhof, "Generalized gradient approximation made simple," Phys. Rev. Lett. **77**(18), 3865 (1996).
[46]I. J. Park, S. Kwon, and R. K. Lake, "Effects of filling, strain, and electric field on the Néel vector in antiferromagnetic CrSb," Phys. Rev. B **102**(22), 224426 (2020).
[47]G. Yang, Z. Li, S. Yang, J. Li, H. Zheng, W. Zhu, Z. Pan, Y. Xu, S. Cao, W. Zhao, A. Jana, J. Zhang, M. Ye, Y. Song, L. H. Hu, L. Yang, J. Fujii, I. Vobornik, M. Shi, H. Yuan, Y. Zhang, Y. Xu, and Y. Liu, "Three-dimensional mapping of the altermagnetic spin splitting in CrSb," Nat. Commun. **16**(1), 1442 (2025).
[48]J. Ding, Z. Jiang, X. Chen, Z. Tao, Z. Liu, T. Li, J. Liu, J. Sun, J. Cheng, J. Liu, J. Sun, J. Cheng, and D. Shen, "Large band splitting in *g*-wave altermagnet CrSb," Phys. Rev. Lett. **133**(20), 206401 (2024).
[49]S. Reimers, L. Odenbreit, L. Šmejkal, V. N. Strocov, P. Constantinou, A. B. Hellenes, R. J. Ubiergo, W. H. Campos, V. K. Bharadwaj, A. Chakraborty, T. Denneulin, W. Shi, R. E. Dunin-Borkowski, S. Das, M. Kläui, J. Sinova, and M.

11 February 2026 02:08:35

Published under an exclusive license by AIP Publishing

Jourdan, "Direct observation of altermagnetic band splitting in CrSb thin films," Nat. Commun. **15**(1), 2116 (2024).
[50]M. Zeng, M. Y. Zhu, Y. P. Zhu, X. R. Liu, X. M. Ma, Y. J. Hao, P. Liu, G. Qu, Y. Yang, Z. Jiang, K. Yamagami, M. Arita, X. Zhang, T.-H. Shao, Y. Dai, K. Shimada, Z. Liu, M. Ye, Y. Huang, Q. Liu, and C. Liu, "Observation of spin splitting in room-temperature metallic antiferromagnet CrSb," Adv. Sci. **11**(43), 2406529 (2024).
[51]D. F. Shao, Y. Y. Jiang, J. Ding, S. H. Zhang, Z. A. Wang, R. C. Xiao, G. Gurung, W. J. Lu, Y. P. Sun, and E. Y. Tsymbal *et al.*, "Néel spin currents in antiferromagnets," Phys. Rev. Lett. **130**(21), 216702 (2023).

11 February 2026 02:08:35

Published under an exclusive license by AIP Publishing